Earth and Planetary Science Letters 499 (2018) 83–94

Contents lists available at ScienceDirect

Earth and Planetary Science Letters

www.elsevier.com/locate/epsl

Quantifying the missing sink for global organic carbon burial during a Cretaceous oceanic anoxic event

Jeremy D. Owens [a,*], Timothy W. Lyons [b], Christopher M. Lowery [c]

[a] Department of Earth, Ocean and Atmospheric Science, National High Magnetic Field Laboratory, Florida State University, Tallahassee, FL 32306, USA
[b] Department of Earth Sciences, University of California, Riverside, CA 92521, USA
[c] Institute for Geophysics, The University of Texas at Austin, Austin, TX 78758, USA

ARTICLE INFO

Article history:
Received 16 February 2018
Received in revised form 14 July 2018
Accepted 16 July 2018
Available online xxxx
Editor: D. Vance

Keywords:
oceanic anoxic event
global organic carbon distribution
carbon map
redox
ArcGIS

ABSTRACT

The Cretaceous experienced numerous global and local climatic perturbations to the ocean–atmosphere system, especially during periods of known widespread organic-carbon burial termed oceanic anoxic events (OAEs). The Cenomanian–Turonian boundary event (~93.9 Ma), or OAE-2, is the best documented and widespread organic carbon (OC) burial event in Earth history—with more than 170 sections published. Despite the substantial number of locations, the majority is found within the proto-Atlantic Ocean, Tethys Ocean and epicontinental seaways. It has been hypothesized that the pervasive burial of OC during OAE-2 caused the observed positive carbon isotope excursion (2 to 7‰, average ~3‰). The isotope excursion can help constrain the global burial of OC, even for unstudied portions of the global ocean. This approach can solve for 'missing' OC sinks by comparing model estimates with the known distribution of OAE-2 sediments and their OC contents. Specifically, mapping the known spatial extent of OC burial in terms of mass accumulation rates (MARs), and comparing those results with the prediction using a forward box model to derive the amount of OC burial to reproduce the globally observed positive carbon isotope excursion. The available OC data from outcrop and drill core, with reasonable extrapolation to analogous settings without data, quantifies ~13% of the total seafloor, mostly from marginal marine and epicontinental/epeiric settings. However, this extrapolation for OC burial, plus using most appropriate MARs to unknown portions of the seafloor, fail to account for the amount of OC burial predicted for a 3‰ positive carbon isotope excursion. This discrepancy remains even when considering additional sinks of organic carbon burial such as coal, lacustrine environments, authigenic carbonate, and the loss of OC associated with hydrocarbon reservoirs. This outcome points to a large reservoir of OC that is not currently constrained, such as highly productive margins and/or equatorial regions, or a small but significant increase deep ocean OC burial. Another possibility is that the carbon fluxes are less than those used in the model which would require less OC burial to explain a ~3‰ carbon isotope excursion.

1. Introduction

Extensive deposition of organic-rich facies was common throughout the Mesozoic era; in the Cretaceous, these time intervals have aptly been named oceanic anoxic events (OAEs) (Schlanger and Jenkyns, 1976). The Cenomanian–Turonian boundary event (93.9 Ma), or OAE-2, is the most extensively studied of these events, with reports of elevated organic carbon (OC) preservation in multiple ocean basins (Indian, Pacific, Atlantic and Tethys oceans; Fig. 1A) and under various paleo-water depths, paleolatitudes and depositional conditions (Arthur et al., 1987; Jenkyns, 2010; Kuroda and Ohkouchi, 2006; Schlanger et al., 1987; Takashima et al., 2006). Due to the enhanced burial of organic matter, which preferentially sequesters isotopically light carbon, there is a coeval positive carbon isotope ($\delta^{13}C$) excursion (Schlanger et al., 1987; Scholle and Arthur, 1980). Importantly, the positive carbon isotope excursion is observed in all carbon phases: organic-C, carbonate-C and terrestrial OC (as reviewed in Jenkyns, 2010). The magnitude of this excursion recorded in marine organic and carbonate carbon ranges between ~2 and ~7‰ with an average of ~3‰ (Fig. 1B; Erbacher et al., 2005; Jarvis et al., 2006; Schlanger et al., 1987). The larger isotope excursion (~7‰) for the organic carbon record has been interpreted to reflect a changing net fractionation between organic matter and inorganic C over the course of the event, possibly due to declining atmospheric pCO_2 (Kump and Arthur, 1999). Also, much of the $\delta^{13}C_{organic}$

* Corresponding author.
E-mail address: jdowens@fsu.edu (J.D. Owens).

https://doi.org/10.1016/j.epsl.2018.07.021
0012-821X/

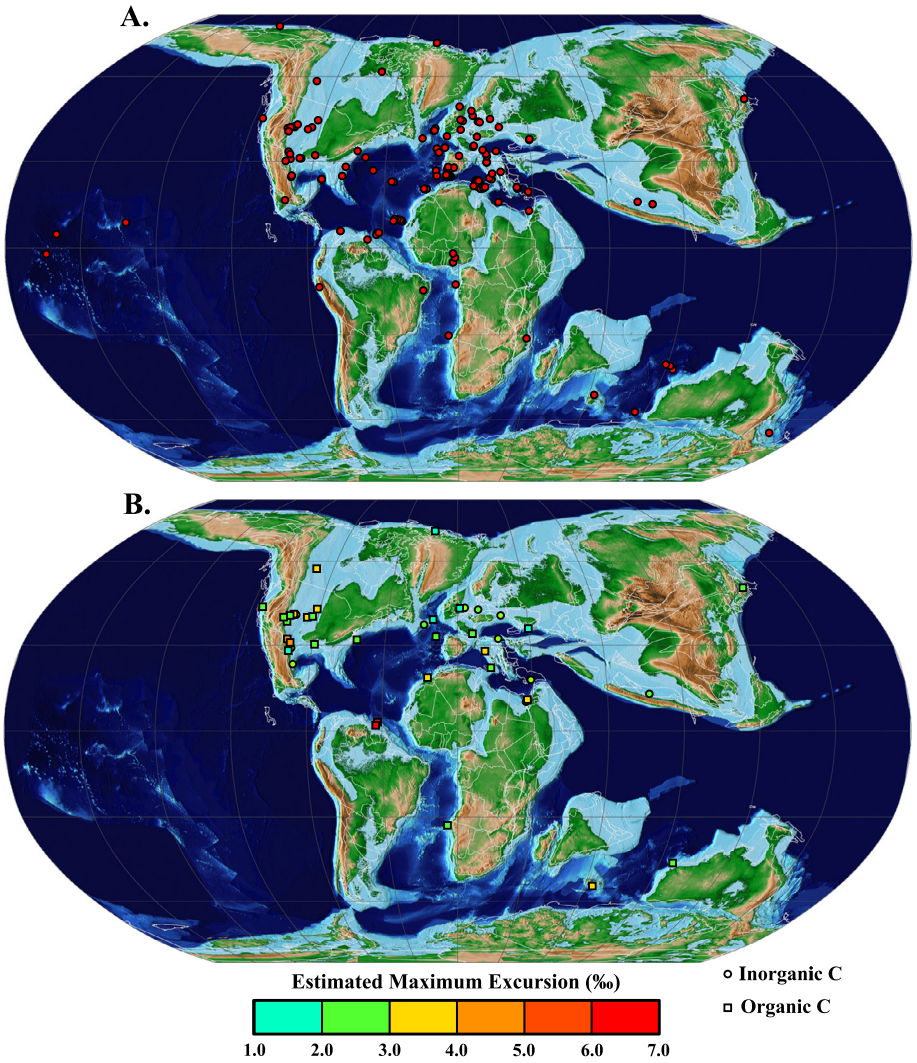

Fig. 1. Fig. 1A shows the localities that have been documented to contain OAE-2 sediments. Fig. 1B documents the maximum carbon isotope excursion globally with squares represent an excursion in organic carbon and circles document inorganic carbon perturbation. This map is adapted from the PALEOMAP Project (Scotese, 2008). (For interpretation of the colors in the figure, the reader is referred to the web version of this article.)

variation recorded globally can be attributed to varying paleolatitudinal gradients in sea surface temperature, with increased fractionation at lower latitudes (van Bentum et al., 2012). The pervasive OC burial inferred from the isotope excursion during OAE-2 is thought to be the result of either enhanced productivity or preservation, due to increased anoxia, and/or a combination of these two factors (Kuypers et al., 2002; Schlanger et al., 1987; Schlanger and Jenkyns, 1976).

OAE-2 is characterized by an overall warm climate recorded in proxy records for elevated temperatures (Jarvis et al., 2011; Takashima et al., 2006) likely related to high pCO_2 (estimated to be 2–8 times higher than the present level; Barclay et al., 2010; Takashima et al., 2006) and increases in sea level (Jarvis et al., 2001). However, proxy evidence also points to climatic cooling during the OAE, referred to as the Plenus cold event, which has been attributed to the widespread burial of OC and a concomitant decrease in atmospheric pCO_2 (Jarvis et al., 2011; van Bentum et al., 2012). Sustaining enhanced productivity, export and burial of OC throughout the event requires increased delivery of nutrients (e.g., N and P) and bio-essential metals (e.g., Fe) to the surface ocean. Increased seafloor spreading rates (Jones and Jenkyns, 2001), increased weathering (Pogge von Strandmann et al., 2013) and/or enhanced phosphorus regeneration under oxygen-deficient marine conditions (Mort et al., 2007; Van Cappellen and Ingall, 1994) have all been implicated in explaining enhanced availability of nutrients. Various geochemical data point to increased volcanism during OAE-2 associated with the emplacement of large igneous provinces (e.g., Du Vivier et al., 2015; Turgeon and Creaser, 2008), which could explain high pCO_2 values and may have fostered enhanced delivery of bio-essential metals such as iron to the oceans. An important consideration, however, is the difficulty in transporting dissolved and other bioreactive forms of iron in seawater under both oxic and anoxic-sulfidic (euxinic) conditions (Owens et al., 2012).

Traditionally, the widespread distribution of organic-rich sediments has been used to infer regional and even global extents of anoxic deposition, which can enhance preservation and thus burial (Schlanger et al., 1987; Takashima et al., 2006), but is not a direct proxy for marine oxygen content (e.g. Them et al., 2018). Thus, numerous geochemical proxies have been applied to OAEs to independently constrain local anoxia and/or euxinia (Brumsack, 2006; Hetzel et al., 2011; Ostrander et al., 2017; Owens et al., 2017, 2016; van Bentum et al., 2009; Zhou et al., 2017; and additional references within all), including evidence for photic zone euxinia based on organic biomarker data (Kuypers et al., 2002; van Bentum et al., 2009). Nevertheless, the documented global record of local redox conditions remains poor during OAE-2—especially in the Pacific, Indian and Arctic oceans. Recent studies have suggested widespread reducing, low oxygen but non-

euxinic bottom waters prior to the event (Ostrander et al., 2017; Owens et al., 2016), with euxinic deposition occurring at the onset of the OAE (Dickson et al., 2016b; Owens et al., 2013). The global pervasiveness of reducing conditions has a dramatic effect on trace metal availability, with decreasing sediment concentrations and implied seawater inventories captured at several localities during OAE-2, possibly affecting the nitrogen cycle and primary production (as reviewed in Owens et al., 2016). Importantly, organic carbon preservation is also tightly coupled to sedimentation rate (Canfield, 1994), although other factors can also contribute to this relationship (e.g., Hartnett et al., 1998).

Understanding the global extent of carbon burial throughout the Phanerozoic has important implications for time-varying atmospheric pO_2 and pCO_2 contents (Berner and Canfield, 1989). While estimates for OC burial are traditionally derived by coupling mass balance modeling of C-isotope archives for dissolved inorganic carbon in seawater (Kump and Arthur, 1999), Berner and Canfield (1989) utilized took a different approach—similar to one employed here. Specifically, these authors estimated OC burial through the Phanerozoic using abundances of the major sedimentary rock types for given time intervals and their average total organic carbon (TOC) contents (e.g., Ronov, 1976). Using OC burial, Berner and Canfield (1989) could reproduce the results derived from model assessments of the long-term carbon isotope curve. Because their focus was long-term estimates for atmospheric O_2 and CO_2, they omitted short-term episodes such as OAEs, but two studies have attempted a reconstruction of OC burial for short-term Cretaceous climate events using the general stratigraphic record (Föllmi, 2012; Westermann et al., 2010). In our study of OAE-2, we have constructed a global map of OC accumulation based on an extensive literature compilation of the sediments spanning this interval. These measured values were then extrapolated to un-sampled portions of the ocean for regions proximal to the available data and of similar depositional setting, with the goal of reasonably expanding the amount of 'known' seafloor (similar to the method used by Jahnke, 1996). By comparing our isotope model and the mapped distributions of TOC in OAE-2 sediments, we can predict the magnitude of additional OC burial required to explain the observed carbon isotope excursion.

2. Methods

2.1. Estimating global carbon burial from known sediment distributions

Our estimates of global OC burial during the OAE interval begin with calculations of average mass accumulation rates (MAR; g/cm^2/kyr) for each location. This step requires an understanding of the local sedimentation rate (cm/kyr) and the rock density (g/cm^3), as well as average TOC content (wt%). Mean sedimentation rate over the event was calculated using the reported thickness of the OAE interval and an estimated event duration of 500 kyr. Event duration has been estimated previously using numerous sections and methods—yielding a range between 450 and 900 kyr (as reviewed in Eldrett et al., 2015). We chose 500 kyr for the overall estimated duration. However, because we assume the same duration in all our calculations for both methods used in this study, any reasonable variation in that estimate will not affect our fundamental conclusions. The sediment thickness of the OAE for each section was determined using the positive $\delta^{13}C$ excursion expressed in either organic and/or inorganic carbon (both data types are not generally available) or biostratigraphic estimates and assumes continuous deposition. The initiation and termination of the event are defined by the initial rise above pre-event baseline values and the subsequent return, respectively. We assume a constant rock density (g/cm^3) of 2.4 because of the commonly high OC contents, rather than the typical value of ~2.7 applied to various sedimentary mixtures of silicate and carbonate minerals. Use of different rock densities has minimal effect on our results and interpretations (see discussion below). Unfortunately, numerous OAE-2 sections were excluded from our compilation because they lacked either sufficient TOC data and/or the $\delta^{13}C$ context needed to determine the thickness of the interval. The average TOC values may include terrestrial material, but a few sites suggest the organic matter is dominantly of marine origin (Hasegawa et al., 2013; Keller et al., 2001; Kolonic et al., 2005). Furthermore, this compilation did not discriminate between organic matter types because the overall goal is to quantify the total amount of organic carbon burial during the event and its relationship to the carbon isotope excursion, irrespective of the primary source.

To best reproduce the global distribution of sites documented to contain OAE-2, we used PaleoAtlas® with ArcGIS® and PointTracker® to reconstruct the most accurate paleo-locations (latitude and longitude). Specifically, we converted modern GPS data (some estimated using Google® Maps) to ancient locations through known plate movements from ~90 Ma (Scotese, 2008). It should be noted that two sites (supplemental information site numbers 20 and 171) have paleo-location uncertainties due to being on the edge of the reconstructed plate boundary. The exact location of these two sites does not affect our fundamental conclusions. The average TOC, sediment thickness, sedimentation rates and OC MAR for each point during the OAE can be found in Table 1. Also included in Table 1 are 'polygon estimates.' Polygons are the areas over which the OC data from single ($n = 20$) or multiple locations ($n = 18$) are extrapolated. The single-site OC MAR, or averages from multiple sites, are extended to define broader depositional areas around those points, as dictated by roughly similar paleowater depths and thus inferred similarities in depositional setting. Those assumed similarities include sedimentation rate and primary production. There are obvious limitations to this approach but, in a first-order sense, it should be possible to capture the basic patterns of global OC burial. There are exceptions, however, in that most of the ancient deep ocean remains uncharacterized. The uncertainty in such cases is large, particularly given the very few data in regions like the Pacific Ocean. Furthermore, the Pacific Ocean sites represent bathymetric highs. It is reasonable to use modern oceanographic dynamics for OAE-2, as ocean interiors (central gyre regions) are typified by low primary production. However, zones of divergence in the surface ocean, such as the modern equatorial upwelling zones, represent likely exceptions. Because we aimed to avoid over-extrapolation of data to unknown regions, conditions in many coastal regions remain mostly conjectural but are potential sites of appreciable OC burial.

2.2. Carbon isotope model

We constructed a forward box model for the global carbon cycle to quantify the amount of OC burial required to drive the observed carbon isotope excursion. Initial boundary conditions were prescribed based on previously estimated values for a greenhouse world (Kump and Arthur, 1999) and individual parameters were perturbed to recreate the observed isotopic event relative to the pre-event baseline.

The following time-dependent expression was used to model the isotopic composition of carbon (see Kump and Arthur, 1999):

$$\frac{\partial \delta_0}{\partial t} = \frac{F_w(\delta_w - \delta_0) - F_{carb}\delta_{carb} - F_{org}\Delta C}{M_0},$$

where M_0 is the initial concentration of dissolved inorganic carbon (DIC) in the marine reservoir and δ_0 is the initial isotopic composition. The input to the ocean comprises the combined fluxes delivered from continental weathering and volcanic emis-

Table 1
Relevant data for each polygon from Fig. 4, which includes the compiled thickness and average TOC from the literature. The sedimentation rate and OC MAR were calculated as discussed in the text. The area for each polygon was calculated using ArcGIS®, and the amount of OC buried for each polygon was calculated by multiplying the area and the OC MAR average for the polygon.

Polygon ID	Paleo water depth	Total sections (n)	Average thickness (m)	Average TOC (wt%)	Average sedimentation rate (cm/kyr)	OC MAR (g/cm^2/kyr)	Area (10^8 km^2)	Area (%)	OC burial during OAE 2 (10^{18} g)
0	Margin	1	33.00	3.45	6.60	0.55	0.003	0.087	0.88
1	Margin	1	265.00	1.25	53.00	1.59	0.008	0.224	6.58
2	Margin	17	8.44	2.35	1.69	0.08	0.044	1.182	1.73
3	Margin	1	0.40	3.00	0.08	0.01	0.023	0.635	0.07
4	Margin	1	142.00	0.50	28.40	0.34	0.006	0.151	0.95
5	Margin	1	12.00	5.40	2.40	0.31	0.006	0.157	0.90
6	Margin	1	3.92	3.83	0.78	0.07	0.009	0.230	0.31
7	Margin	2	0.85	7.04	0.17	0.03	0.007	0.200	0.11
8	Margin	1	1.20	22.00	0.24	0.13	0.004	0.098	0.23
9	Margin	2	0.60	1.60	0.12	0.00	0.006	0.162	0.01
10	Margin	2	10.10	3.00	2.02	0.07	0.009	0.252	0.32
11	Margin	2	2.50	1.00	0.50	0.01	0.017	0.452	0.10
12	Margin	2	0.40	9.00	0.08	0.02	0.006	0.170	0.05
13	Margin	1	0.50	10.00	0.10	0.02	0.002	0.053	0.02
14	Margin	1	21.00	1.13	4.20	0.11	0.004	0.113	0.23
15	Margin	2	1.50	1.20	0.30	0.01	0.009	0.241	0.04
16	Margin	1	1.67	6.37	0.33	0.03	0.007	0.178	0.11
17	Margin	3	3.50	1.00	0.70	0.02	0.069	1.864	0.58
18	Margin	1	0.50	5.80	0.10	0.01	0.011	0.305	0.08
19	Mixed	3	0.27	4.93	0.05	0.01	0.020	0.538	0.06
20	Margin	4	1.15	8.45	0.23	0.05	0.003	0.074	0.07
21	Margin	6	2.43	24.37	0.49	0.23	0.006	0.171	0.73
22	Margin	4	31.75	8.13	6.35	1.24	0.003	0.080	1.83
23	Margin	5	4.95	5.44	0.99	0.11	0.002	0.067	0.14
24	Margin	47	24.70	1.72	4.94	0.22	0.007	0.183	0.74
25	Abyssal	1	7.00	1.25	1.40	0.04	0.023	0.632	0.49
26	Margin	1	15.00	0.50	3.00	0.04	0.009	0.254	0.17
27	Mixed	5	124.00	4.00	24.80	2.15	0.017	0.463	18.37
28	Abyssal	2	0.25	9.60	0.05	0.01	0.043	1.165	0.25
29	Margin	1	5.00	2.50	1.00	0.06	0.008	0.224	0.25
30	Margin	2	2.85	14.75	0.57	0.21	0.006	0.176	0.69
31	Margin	3	6.00	3.03	1.20	0.10	0.006	0.157	0.29
32	Margin	1	40.00	1.00	8.00	0.19	0.002	0.066	0.23
33	Margin	1	6.50	11.61	1.30	0.36	0.008	0.217	1.45
34	Margin	1	0.15	10.50	0.03	0.01	0.035	0.956	0.13
35	Margin	1	4.10	4.38	0.82	0.09	0.007	0.193	0.31
36	Margin	1	30.00	0.40	6.00	0.06	0.019	0.527	0.56
37	Margin	1	7.00	5.50	1.40	0.18	0.007	0.188	0.64

Mapped with data

	Area weighted average thickness (m)	Area weighted average TOC (wt%)	Area weighted average sedimentation rate (cm/kyr)	Area weighted OC MAR (g/cm^2/kyr)	Area (10^8 km^2)	Area (%)	OC burial during OAE 2 (10^{18} g)
Margin total	12.61	3.60	2.52	0.11	0.38	10.3	21.52
Abyssal total	2.08	6.26	0.42	0.02	0.09	2.3	0.79
Mixed total	124.00	4.00	24.80	2.15	0.02	0.5	18.37
Total area with data					0.48	13.1	40.69
Total ocean area					3.69	100.0	

Lacks data

Margin total					0.46	12.5	
Abyssal total					2.75	74.5	

sions (F_w). These input fluxes can be combined because their isotopic compositions are similar—defined as δ_w (Kump and Arthur, 1999). The output fluxes are the burial of carbonate carbon (F_{carb}) and OC (F_{org}), with only OC having the capacity for substantial isotopic fractionation of the marine DIC reservoir. The ΔC is the isotopic fractionation associated with primary production—that is, the isotopic difference between organic carbon and the reservoir of DIC. The carbonate isotope fractionation is held constant and approximated at zero, implying that carbonate precipitation initially captures the isotopic composition of seawater DIC.

The starting reservoir concentration, isotopic estimates and fluxes shown in Table 2 are based on a high pCO_2 Cretaceous world with an elevated DIC pool (similar to Kump and Arthur, 1999; Kuroda and Ohkouchi, 2006). These assumptions equate to a doubling of the modern inputs and outputs, and an increased ocean reservoir (DIC). We can also explore the amount of OC needed to drive the magnitude of the excursion using these parameters and compare to modern values. In our effort to simulate the 3‰ fractionation in a high pCO_2 world, we assumed an initial DIC reservoir of 45.6×10^{18} g (referred to as exagrams or Eg herein) of C (M_0) [double modern value], with a starting isotopic

Table 2
Initial parameters for the C box model. All flux values are for millions of years (Myr). The isotopic fractionation imparted by inorganic carbon is negligible and is not included in this model (similar to Gill et al., 2011; Kump and Arthur, 1999; Kurtz et al., 2003), and values in parentheses were used in the modern flux comparison (Kurtz et al., 2003).

	Initial marine reservoir	Weathering flux	Organic carbon burial flux	Inorganic carbon burial flux
Concentration (10^{18} mol/Myr)	3.8 (3.3)	50 (25)	10 (5)	40 (20)
Concentration (10^{18} g/Myr)	45.6 (39.6)	602 (301)	120 (60)	482 (241)
δ^{13}C (‰)	+1.7	−4.0	−28	–

value of 1.7‰ (δ_0). The input of carbon from weathering was assigned a flux of 601 Eg of C per Myr (F_w) with an isotope value of −4.0‰ (δ_w). The OC burial flux was 60.2 Eg of C per Myr (F_{org}) assuming an OC fractionation of −28‰ (ΔC: the estimated fraction for the Cretaceous; Hayes et al., 1999) and carbonate burial flux of 40 Eg of C per Myr—unfractionated from the DIC reservoir. These increased input, output and reservoir values allow the model to begin at steady state prior to perturbations.

We used a sensitivity test to examine our results in terms of several important parameters: OC burial, starting marine concentration, OC fractionation, the weathering/volcanic input flux and carbonate burial. For example, we varied the amount of OC burial from 60.1 to 100.3 Eg of C for the 500-kyr OAE to observe the magnitude of the isotopic excursion, while holding all other variables constant. The sensitivity tests include varying the DIC reservoir size from 75% to 125% of the initial assumed value (45.6 Eg of C), changing the OC isotope fractionation from −28 to values of −26 and −30, varying the weathering fluxes from 96% to 200% of the starting value (602 Eg of C per Myr) and varying the carbonate burial flux from 25% to 105% of the initial value (482 Eg of C per Myr).

3. Results

3.1. Global carbon burial estimates from sediment distributions

The global distribution of sampled OAE-2 sites (Fig. 1A) is dominated by the Tethys and proto-North Atlantic oceans. The many ocean drilling sites are complemented by outcrop samples, mostly from Europe, northern Africa and North America. Our map is similar to other compilations (Takashima et al., 2006; Trabucho Alexandre et al., 2010)—with the same sample biases. Of these 172 sites, there are 132 localities with published TOC values and stratigraphic thicknesses for OAE-2, which were used to calculate average TOC and sedimentation rate. Most of the localities (119 sections) were deposited on continental margins and slope settings (hereafter collectively referred to hereafter as 'margins'). The Pacific Ocean is constrained by only five sections, with three of the sites located on margins and two from the equatorial region on bathymetric highs (i.e., seamounts).

Using ArcGIS®, we estimated the total surface area of the ocean to be ~3.69 × 10^8 km^2 during this interval, which is slightly greater than the modern ocean value of 3.61 × 10^8 km^2 (Charette and Smith, 2010). The 38 polygons generated account for ~0.48 × 10^8 km^2 or 13.1% of the ocean surface area. The areas within the polygons are classified as: margins (including epicontinental seas), which constitute a majority of the constrained ocean with 10.3% of the total ocean surface area; abyssal settings (including bathymetric highs in the Pacific) at 2.3%; and sites of mixed bathymetry (comprising both marginal and abyssal contributions impossible to separate into the two depositional environments) at 0.5% (see Table 1). Estimates from mapping indicate that marginal settings make up an additional 12.5% of the ocean surface area. These additional areas unfortunately lack the data necessary to calculate an OC MAR. Thus, marginal marine settings account for a total of ~22.8% of the total ocean seafloor, meaning that more than half of Cretaceous ocean margins are unrepresented in this work. This method has allowed us to estimate only a very small portion of the deep ocean seafloor due to the relatively small number of sample locations. The deep ocean seafloor represents an estimated 76.9% of the total ocean, with only ~2.3% accounted for in the existing OAE-2 data. However, these settings bury only ~10% of the OC in the modern ocean (Burdige, 2007). Assuming similar relationships during the Cretaceous, the missing marginal settings become most important to quantify because of the high associated levels of primary production and subsequent burial.

Of the 132 sections, 78 localities have average TOC values greater than 2 wt% (Fig. 2). Average TOC values for each locality range from 0.1 wt% to 44.5 wt%, and the highest values are located in Italy, the deep ocean off the coast of Spain and the southern portion of the proto-North Atlantic. Fig. 3 shows calculated sedimentation rates, with nearly all sites plotting within the ranges that are typical for analogous depositional settings in the modern ocean (e.g., continental margin and deeper sites proximal to abyssal plains; Sadler, 1981) from 0.03 to 53 (cm/kyr). Thus, the key parameter for our study is OC MAR, as high sedimentation may result in low TOC but very high OC burial during OAE2.

The calculated OC MAR values for each site range from 0.001 to 3.3 (g/cm^2/kyr), with the abyssal plain sites showing some of the lowest values (Fig. 4), while other low values are mostly from carbonate-rich localities with very low TOC contents. Importantly, there are several localities with low TOC values but relatively high OC MARs (i.e., coastal Tarfaya, California and Japan) due to high sedimentation rates and concomitant lithogenic dilution. The colored polygons in Fig. 4 represent average OC MARs for a given area. Because we assume similar conditions within each polygon, each is assigned a single average OC MAR (Table 1). Generally, each polygon represents only one depositional environment: marginal, epicontinental seaway, or deep abyssal, with the notable exceptions of polygons 19 and 27 in the Atlantic Ocean. These two outliers represent transects that include marginal and abyssal environments, but are grouped together in a single polygon due to their relatively similar OC MAR values and the difficulty in delineating the boundaries for each environment. Therefore, these two polygons extend from marginal marine to abyssal environments all the way to the mid-ocean ridge, which likely yields an overestimation for the average OC MAR for both polygons.

The amount of OC buried during the OAE for each polygon can be calculated using the OC MAR, the area for each polygon, and the estimated duration of the OAE, yielding a predicted burial of 41 Eg of C during the OAE for the known 13.1% of the seafloor. As mentioned previously, this compilation is based on an assumed average rock density for all samples of 2.4 (g/cm^3). Changing this value to 2.7 (g/cm^3) increases the estimated OC burial by ~5 Eg during the OAE, for a total known OC burial of 46 Eg. Although speculative, the unknown portions of the ocean, comprising 87% of the seafloor, were assigned OC MAR values using both OAE weighted (by area) average data (not including 'mixed' values) and, for comparison, known modern values from analogous settings, to calculate estimated total OC burial. Specifically, using an OAE OC

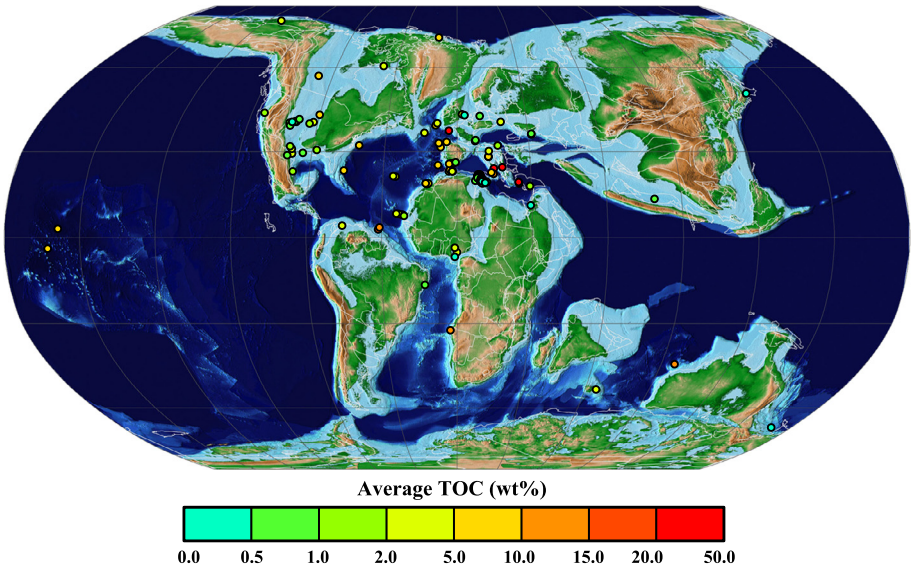

Fig. 2. Localities of all sites with TOC values during OAE-2. This compilation required that the individual sites also contain requisite information to calculate sedimentation rates. This map is adapted from the PALEOMAP Project (Scotese, 2008). (For interpretation of the colors in the figure, the reader is referred to the web version of this article.)

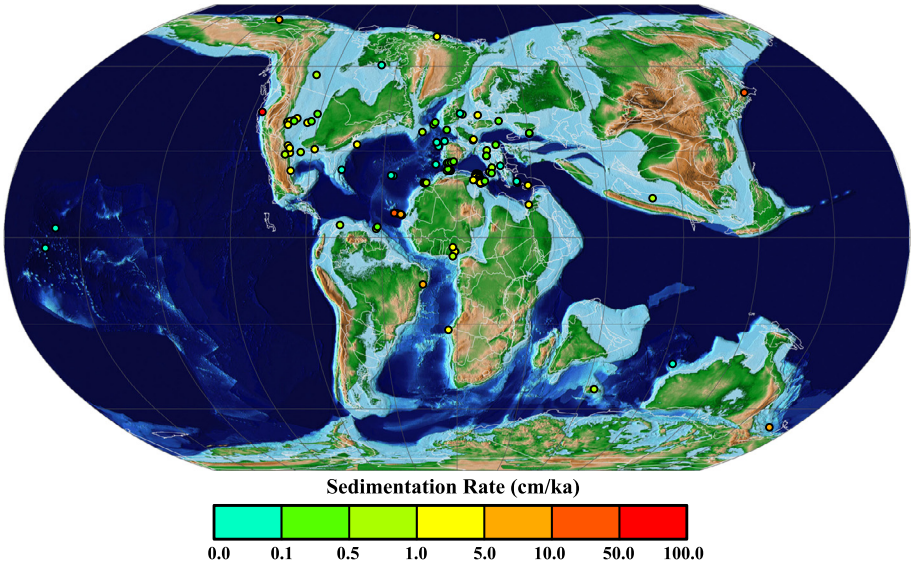

Fig. 3. Sedimentation rate for the global compilation of all localities that also have TOC values. This map is adapted from the PALEOMAP Project (Scotese, 2008). (For interpretation of the colors in the figure, the reader is referred to the web version of this article.)

MAR for the margins, because of indications for elevated values during the event and modern values for the abyssal sites yields an additional ~29 Eg for a total of ~70 Eg of OC during the OAE or nearly 40 Eg more OC burial than in the modern ocean (Tables 1 and 3). Using modern OC burial for the margins dramatically reduces the estimated amount. Further, using the weighted single global average for OAE-2 OC MAR value, which is dominated by marginal settings, for all marine environments would increase the OC burial to ~94 Eg. However, such high OC MAR values for the relatively nutrient poor regions of the central deep oceans are unlikely (discussion below).

3.2. Carbon isotope modeling

The observed carbon isotope trends demand dramatic perturbations to the carbon cycle during OAE-2. To elucidate the implications of the carbon isotope excursion, we constructed a forward box model as described earlier. The model suggests that the magnitude of the excursion is dictated by (1) the amount of OC buried (Fig. 5), (2) the OC fractionation [difference between the DIC pool and the OC value (Fig. 6B)] and (3) the magnitude of the weathering flux (Fig. 6C)—sensitivity to the starting reservoir size (Fig. 6A) and amount of carbonate burial (Fig. 6D) is minimal. The only variable that directly and significantly controls the magnitude of the transient positive excursion is the amount of OC buried—because of its large associated fractionation.

Enhanced OC burial is required to reproduce the large positive excursion, whether using the high pCO_2 scenario or modern values for the carbon reservoir and fluxes. We emphasize the high pCO_2 scenario, which doubles the initial parameters relative to modern inputs, outputs and the starting DIC value (45.6 Eg based on the estimated high levels of atmospheric pCO_2; similar to Kump and Arthur, 1999). Fig. 5 also shows model results assuming modern reservoir and flux relationships, which requires only half the burial of OC compared to the higher, more realistic, pCO_2 scenario.

The initial reservoir size was set prior to the simulation run, but variations in fractionation and weathering were triggered at the onset of the OAE—as current research suggests abrupt weathering

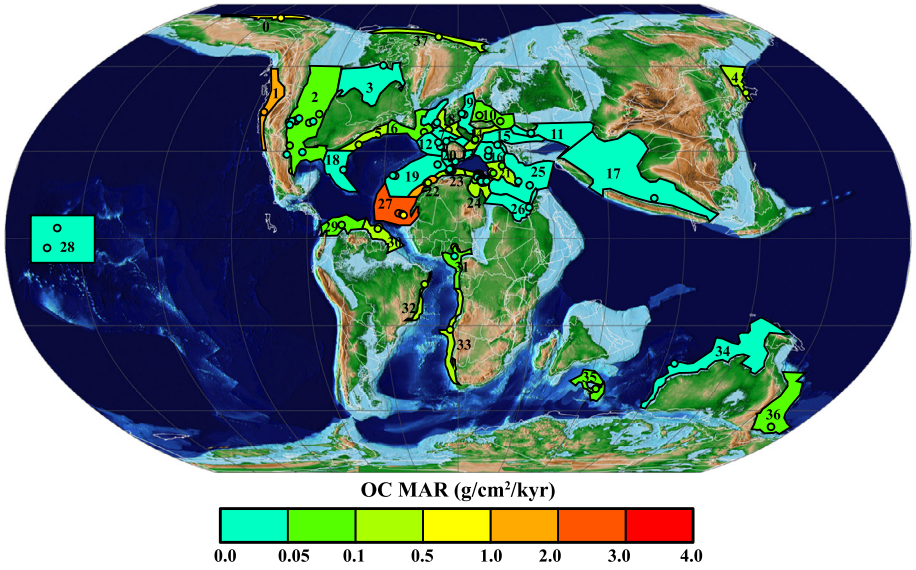

Fig. 4. Global distribution of calculated OC MAR for each locality. Individual circles represent data for each locality and the polygons plotted encompass the average OC MAR for all localities within the polygon. The numbers for each polygon corresponds to Table 2. This map is adapted from the PALEOMAP Project (Scotese, 2008). (For interpretation of the colors in the figure, the reader is referred to the web version of this article.)

Table 3
Chart showing the area (km^2 and %) accounted for with the amount of unknown marginal and abyssal settings. The statistical data from the distribution can be compared to the modern estimates (Burdige, 2007) which are fairly similar in terms of % OC burial and area.

	Depositional environment	Weighted average OC MAR ($g/cm^2/kyr$)	Area (10^8 km^2)	OC burial during OAE (10^{18} g)	Area (%)	OC burial (%)
Mapped with data	Margin	0.11	0.38	21.5	10.3	53
	Abyssal	0.02	0.09	0.8	2.3	2
	Mixed	2.15	0.02	18.4	0.5	45
	Total		0.48	40.7	13.1	
Using modern MAR for unknown	Margin	0.030	0.46	6.9	12.5	63
	Abyssal	0.003	2.75	4.1	74.5	37
	Total		3.21	11.0	87.0	
Using OAE 2 MAR averages for unknown	Margin	0.11	0.46	25.3	12.5	48
	Abyssal	0.02	2.75	27.5	74.5	52
	Total		3.21	52.8	87.0	
Most plausible estimates	$Margin_{accounted}$	0.11	0.38	21.5	10.3	31
	$Margin_{unknown}$	0.11[a]	0.46	25.3	12.5	36
	$Mixed_{accounted}$	2.15	0.02	18.4	0.5	26
	$Abyssal_{accounted}$	0.02	0.09	0.8	2.3	1
	$Abyssal_{unkown}$	0.003[b]	2.75	4.1	74.5	6
	Total		3.69	70.1	100.1	
Modern			3.61	30.1		

[a] OAE 2.
[b] Modern average.

changes near the event boundary (Pogge von Strandmann et al., 2013). An OC burial of 60.1 Eg is required to maintain steady state, which is double the modern burial rate due to the doubling of the starting input fluxes. If all other parameters are held constant throughout the run, generating the observed average C-isotope excursion of 3‰ for a high pCO_2 scenario requires an additional burial of 32.3 Eg for a total of 92.5 Eg of OC burial (Fig. 5). Changing the initial marine DIC reservoir (Fig. 6A) or carbonate burial rate (Fig. 6D) has minimal effect on the magnitude of the marine carbon isotope record but does alter the shape of the curve. However, if the initial DIC reservoir size is set below 34.2 Eg, 75% of (high pCO_2 scenario) the initial value, the burial of OC will completely deplete the DIC reservoir. For instance, 70% (high pCO_2 scenario) of the initial value depletes the reservoir in ~450 ka, but larger decreases in DIC will deplete the reservoir more quickly. Varying the fractionation during the OAE affects the magnitude of the excursion: a −26‰ fractionation yields a 2.4‰ excursion (all other parameters being equal), while a −30‰ fractionation equates to a 3.6‰ excursion (Fig. 6B). Modifying the weathering flux dramatically affects the magnitude and shape of the carbon isotope excursion. Doubling the weathering flux can cause a negative 1.2‰ excursion, even with enhanced OC burial during the event (Fig. 6C). Further, a decrease below 96% of 602 Eg of C (the initial starting value) for weathering will completely deplete the DIC reservoir just prior to the termination of the OAE during enhanced OC burial. Lastly, varying carbonate burial (Fig. 6D) at the onset of the event from 25% to 105% of 482 Eg of C (the initial starting value) does not have a significant effect on the isotope excursion but changes the shape of the curve dramatically. Increasing carbonate burial beyond 105% of the initial carbonate burial will completely deplete the DIC reservoir prior to the termination of the OAE.

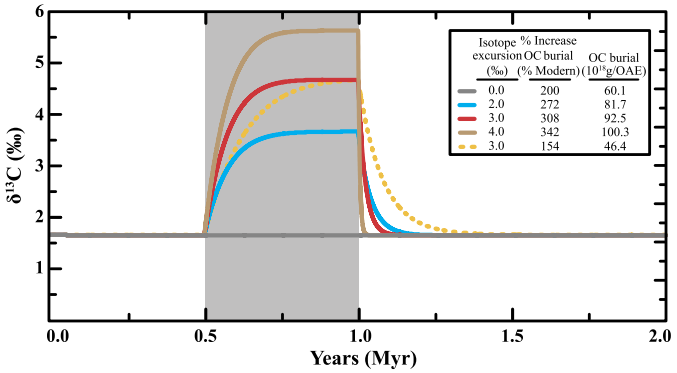

Fig. 5. Modeled OC burial sensitivity test generating a given positive carbon isotope excursion over two million of years (Myr). Demonstrates increased organic carbon burial with the enhanced pCO_2 scenario; the dashed line represents a ~3‰ excursion using modern fluxes (Kurtz et al., 2003).

4. Discussion

4.1. Global carbon burial estimates from sediment distributions

The global distribution of TOC contents during OAE-2 documents a wide range of values, with some of the highest concentrations known from the geologic record (in excess of 45 wt% from DSDP Site 367 – not included due to incomplete core recovery; Kuypers et al., 2002), but the vast majority of the samples have TOC contents less than 10 wt%. Generally, the highest TOC values are located offshore in marginal marine settings, likely in upwelling areas. The distribution of sedimentation rates recorded during OAE-2 also shows a large range but is consistent with other estimates for modern and ancient sedimentation at other times in Earth history (Sadler, 1981). Not surprisingly, the sedimentation rates for OAE-2 are generally high for nearshore locations and lower at deeper, abyssal plain locations, which are far removed from riverine/fluvial detrital sources—as they are today.

The calculated OC MAR during the OAE is the key parameter in our investigation as TOC concentrations alone cannot capture the amount of OC burial (see Figs. 2 and 3). Importantly, as discussed above, the rock density used, whether 2.4 or 2.7 g/cm^2, has minimal effect on the value of the OC MAR. Generally, the highest OC MARs coincide with the highest sedimentation rates, but often have lower TOC contents (generally 0.5 to 2 wt%), which suggests that these sites have not experienced low productivity or preservation. Instead, the low TOC contents likely reflect rapid dilution by detrital siliciclastics and/or pelagic carbonate. Conversely, the TOC-rich localities are generally characterized by relatively slow sedimentation, yielding OAE-2 intervals that are only a few tens of centimeters to meters thick. These thin units preserve a relatively small amount of the total OC buried, when viewed on a global scale using OC MARs. An example of such relationships can be seen at Demerara Rise ODP Site 1258, where TOC values increase during the event likely due to a decrease in carbonate contents (Owens et al., 2016).

OAE-2 is the most extensively documented event among major OC perturbations in geologic history, yet substantial portions of the oceans remain under sampled. The majority of the data are from marginal marine settings and even those are insufficiently characterized (Figs. 2–4). By analogy, the modern ocean buries nearly 85–90% of its OC on continental margins, which are marked by high primary production and rapid sedimentation, as well as high riverine inputs of terrigenous OC (Burdige, 2007). This relationship may also hold true for OAE-2. Importantly, our comparative approach allows us to test this assumption. Additionally, for OAE-2, as for the modern, we predict elevated OC production for the equatorial region relative to central

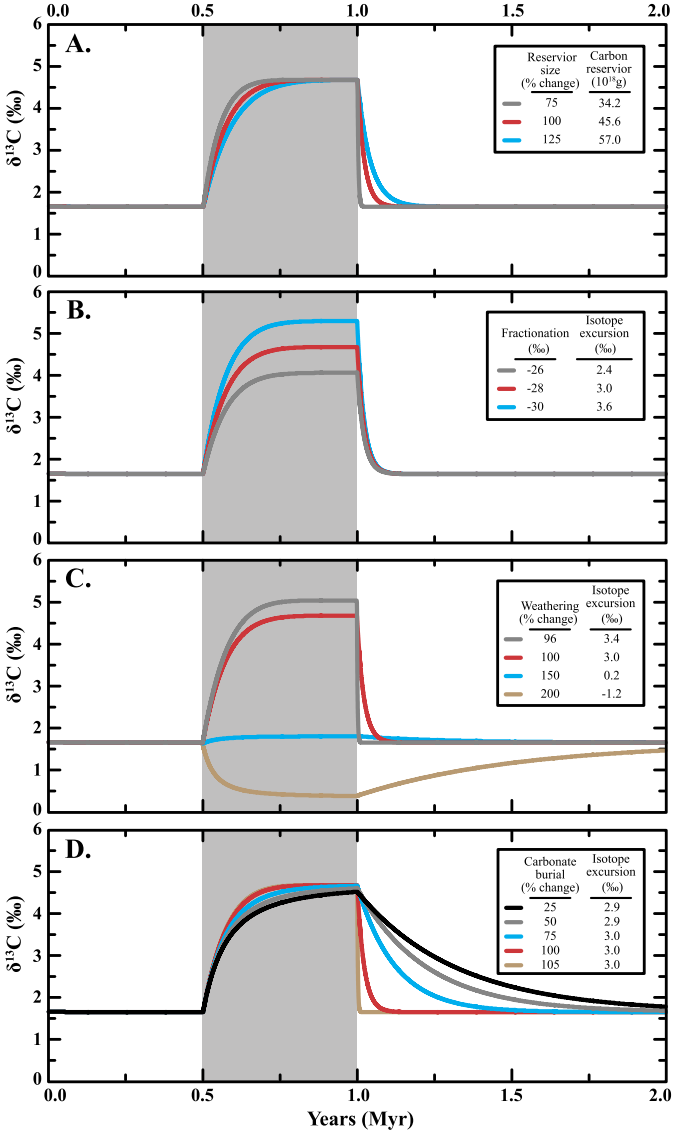

Fig. 6. Modeled sensitivity simulations for reservoir size, OC fractionation weathering flux and carbonate burial variations over two million of years (Myr). Fig. 6A documents the relatively invariant changes in carbon isotopes while increasing the reservoir size. Using the amount OC burial for a 3‰ excursion while varying the OC fractionation which affects the magnitude of the excursion by ~1.2‰ (Fig. 6B). Fig. 6C shows the dramatic effects of varying the weathering flux. Fig. 6D documents the response to varying carbonate burial which has minimal effect on the magnitude of the excursion. Initial parameters (Table 1) for all simulations used an OC burial of 92.5 Eg during the OAE (enhanced pCO_2 scenario).

gyre portions of the open ocean, as well as high preservation given extensive marine oxygen deficiency (Ostrander et al., 2017; Owens et al., 2016)—providing increased potential for OC burial. Importantly, we can account for OC burial beyond that of the entire modern ocean (Burdige, 2007) through accumulation over the 13% of the ocean covered by our OAE-2 extrapolations. We are left with the inevitable conclusion that OAE-2 was a major OC burial event and, based on the observed C-isotope excursion, that vast carbon reservoirs remain unidentified.

4.2. Additional possible OC sinks

Phanerozoic evidence suggests that the dominant sinks of OC lie in the marine environment and large-scale, relatively short-lived, events are most easily tied to marine processes. However, other potentially important sinks should be considered. These

include soil-hosted OC (Berner, 1990), lacustrine OC deposition (Smith, 1990 and references therein), coal deposits (Beerling et al., 2009; Berner and Canfield, 1989), authigenic sedimentary carbonate precipitation (Schrag et al., 2013) and oil migration (Berner, 1990). While the modern sink for soil carbon is relatively large (Jobbágy and Jackson, 2000), substantial variation in OC burial in soils has not been described or predicted during OAE-2. It has been suggested that large lakes might have been dominantly anoxic during OAE-2 and bury large amounts of OC (Smith, 1990). However, to-date there is no record of such processes during OAE-2—in contrast to the Early Jurassic Toarcian OAE (Xu et al., 2017). Furthermore, currently there is no evidence for increased burial of coal during the event (e.g. more OC burial of coal above the background Cretaceous burial). Authigenic carbonate precipitation in pore-fluids has been proposed to be an important sink of ^{12}C-enriched carbon during OC remineralization and/or methane generation (Schrag et al., 2013). However, most sections, especially deeper water facies, show a decline in carbonate contents (Weissert et al., 1998) and there is no current record of very light carbon isotope values recorded in authigenic OAE-2 carbonates. It should be noted that for any of these processes to affect the carbon isotope excursion there would need to be enhanced burial during the OAE, as the 'normal' burial would be included in the numerical modeling as associated total organic carbon burial flux.

Additionally, it is important to consider the amount of OC lost from the known marine sedimentary record as hydrocarbons. Although the volume of hydrocarbons produced during this event is not well documented, recent estimates suggest that since 1870, ~1 trillion barrels of crude oil have been produced from sources of all ages (Jones, 2009), with an estimated reserve of 1.5 trillion barrels of crude oil remaining. In order to account for the maximum amount of OC burial during this event we conservatively assume that all mid-Cretaceous oil is from OAE-2, which is estimated to represent ~29% of all oil produced and in reserve (Klemme and Ulmishek, 1991). Assuming one barrel of crude oil has a mass of 140 kg, which is ~87% carbon by mass, the total estimated amount of OC from all assumed OAE-2 oil is 0.08 Eg of C. Assuming that the OC is not 100% associated with crude oil, but also as shorter chained organic compounds (i.e., straight-chained hydrocarbon with an average of 13 carbon atoms), a total estimate due to unknown amounts of gas production and taking into account the average carbon atoms in various hydrocarbon pools might roughly double this to 0.16 Eg of C. There are obvious uncertainties in these estimates, as there could be natural loss of OC post-burial due to diagenesis, remineralization and/or migration, but the calculated amount of hydrocarbon-related C is negligible relative to the total amount of OC burial needed to generate the observed ~3‰ δ^{13}C excursion.

4.3. Carbon isotope model

The magnitude of the carbon isotope excursion is controlled by the inputs and outputs, and the most important factor is the amount of OC buried, followed by the weathering flux and carbon isotope fractionation linked to photosynthetic production of organic matter from the marine DIC reservoir. It is possible that weathering rates increased, perhaps doubling, at the onset of the OAE (Blumenberg and Wiese, 2012; Jones and Jenkyns, 2001), which would increase the amount of OC burial necessary to achieve a 3‰ excursion. Also, the fractionation factor was held constant for Fig. 5A, although this might be an oversimplification. Limited data suggest that the isotopic offset decreased during the event from −28‰ to −26‰ (Kump and Arthur, 1999 and references therein), which would increase the required amount of OC burial to reach a 3‰ excursion. Variations in the isotopic fractionation during the event could be due to decreased atmospheric pCO_2 linked to increased OC burial (Arthur et al., 1988), reduced volcanogenic CO_2, or changes in ecological communities (Leckie et al., 2002). In fact, recent biomarker evidence points to ecological variation tied to metal limitation during the event (Owens et al., 2016), but the global reach of such effects remains unexplored. A shift to a larger fractionation factor or to less weathering would decrease the total global burial of OC needed to produce the same magnitude carbon isotope excursion. All of these parameters remain fodder for exciting future research, but none clouds our overarching conclusions about high, overwhelmingly unconstrained, marine deposition of OC during OAE-2.

4.4. Implications

Our two approaches yield independent estimates for the amount of OC buried during OAE-2. The global mapping exercise, which accounts for 13% of the ocean, yields an estimated 41 Eg of OC for the duration of the event. This is roughly 133% greater than the amount buried in the entire modern ocean over an equivalent time interval (Table 3). There is a wide range of possible OC burial scenarios for the remaining 87% of the ocean. Using modern MARs for the unknown 87% of the ocean provides an additional 10 Eg of OC, yielding a total of 51 Eg. However, box modeling for a high pCO_2 scenario requires ~60 Eg just to maintain steady state. On the high end, using an OAE average MAR, which likely overestimates the poorly constrained OC burial in the ocean gyres, gives an additional 53 Eg of C for a total of 94 Eg of C (Table 3). With this amount of OC burial, the model-predicted excursion would be ~3.6‰. However, it is more plausible that the margins experienced average OAE OC MAR for known margins, and abyssal plain OC burial was similar to modern values or slightly elevated, as it is difficult to sustain high productivity and bury massive quantities of OC in the relatively nutrient-poor open ocean gyres. Taking this approach provides an additional 29 Eg of C for a total of 70 Eg, which is equivalent to a ~1‰ excursion.

To produce the observed ~3‰ excursion, the box modeling requires a total of 92.5 Eg of C using the high pCO_2 scenario. The mapping estimates using OAE-like margins and modern abyssal MARs fall short by 22.5 Eg of C. Thus, the mapped distribution still leaves significant OC burial unexplained. Increased weathering and/or smaller OC fractionation would require even greater amounts of OC burial to account for the observed carbon isotope excursion.

We are left speculating about the poorly known, potentially highly productive, margins around the Pacific, Indian, Southern and Arctic Oceans. Given that assigning the unknown margins with OAE-2 margin MARs does not account for the necessary OC burial, there must be areas with even higher total OC burial. The Cretaceous Pacific and Indian Oceans likely had oxygen minimum zones similar to their modern counterparts that extend to distal, equatorial regions, and might have experienced the comparably large MARs of the previously defined 'mixed' environments (this likely encompasses shelf, slope and abyssal OC MARs and which are greater than margin MARs alone), which could have driven the amount of OC burial closer to the box-model predictions for a 3‰ excursion. Importantly, in the modern ocean these regions generally experience high sedimentation rates. Thus, the TOC values could be low and still involve burial of significant large amounts of total OC during the event. This possibility would provide a region with elevated OC MARs (similar to 'mixed' MARs) for the OAE, which could drive the positive excursion and could have occurred at depths greater than those with modern high accumulation of OC (Bralower and Thierstein, 1987). From these results, we suggest that unknown portions of the OAE-2 ocean, if sampled, could reveal elevated OC MARs, similar to those of the 'mixed' values, but these environments would likely be restricted to marginal marine

and equatorial upwelling regions—potentially the most productive portions of the ocean that also experience elevated sedimentation rates. The modern oxygen minimum zone impinges on 6.89 $\times$ 10^5 km^2 of sediment in the Pacific Ocean (Helly and Levin, 2004), and using the 'mixed' OC MAR provides an additional 7.5 Eg of C. Thus, a tripling of ocean floor sediment area underlying the modern Pacific Ocean oxygen minimum zone is required to attain a burial of 92.5 Eg of C for a 3‰ C-isotope excursion. Importantly, an increase in OC MARs may not appear now as an "organic-rich shale", given the dilution effects of high bulk sedimentation rates (see Fig. 4).

Generally, the burial of OC and trace metals is linked (Algeo and Lyons, 2006). Thus we can speculate on the potential mechanism for the observed trace metal drawdown during OAE-2 (as reviewed in Dickson et al., 2017; Owens et al., 2016)—particularly for molybdenum (Mo)—by using the amount of OC burial estimated from our box modeling. The Mo/TOC relationship is well characterized for euxinic settings (Algeo and Lyons, 2006; Scott and Lyons, 2012). For example, the Mo-depleted, highly restricted Black Sea shows an average Mo/TOC value of ~7.4, compared to ~19.3 for the Mo-replete, more open Cariaco Basin. The average globally recorded Mo/TOC value for OAE-2 is ~6.5 (Owens et al., 2016).

The OC burial required to explain the observed C-isotope excursion is generally presumed to have been deposited under reducing environments (anoxic and/or euxinic), consistent with the global increase in such settings estimated independently (Dickson et al., 2016b; Ostrander et al., 2017; Owens et al., 2013, 2016). The increased amount of OC burial needed to explain the ~3‰ isotope excursion is 32.4 Eg (92.5 minus 60.1 Eg). Further, a previous estimate argues for a 90% drawdown of the Mo reservoir (Owens et al., 2016). Using this estimate, total Mo burial during OAE-2 can be calculated using a modern seawater concentration of 104 nM (dominantly riverine; as reviewed in Miller et al., 2011), which is equivalent to a total marine reservoir of 14 Pg (10^{15}) of Mo. Further, inputs of 3.1 $\times$ 10^8 mol/yr (dominantly riverine; Miller et al., 2011) would yield an additional ~14 Pg of Mo during the event, provided weathering rates does not increase the fluxes. Thus, to maintain near-complete drawdown would require a total burial of ~28 Pg of Mo during the OAE, yielding an average Mo/TOC ratio of ~8.6, which is similar to the global average of ~6.5 determined from many measurements of individual black shales (Owens et al., 2016). From this general agreement we gain independent confidence in our prescribed boundary conditions and the resulting estimates for OC burial during OAE-2. Coincidentally, the Mo/TOC values, both modeled and observed, are close to those observed in the modern, Black Sea, which experiences almost complete loss of Mo in the water column. It is likely that Mo drawdown was indeed a consequence of widespread anoxic/euxinic conditions during OAE-2.

5. Conclusions

Two independent methods, global sedimentary mapping and forward box modeling, elucidate organic carbon burial during OAE-2. While the known global distribution of organic-rich facies accounts for only a small portion of the ocean, it equates to ~40% of the OC burial required to explain the observed C-isotope excursion. Nevertheless, the 'mapped' distribution of OC burial fails to account for all the predicted OC buried, even when the calculated MAR values are extended to the unknown portions of the ocean—including the nutrient-lean central ocean gyres. Accounting for all the "missing" organic carbon deposition requires OC burial MARs more similar to the 'mixed' depositional environments, as these record the highest MARs. This can be accounted for if ~3 times the sediment area underlying oxygen minimum zones in the modern Pacific Ocean occurred during OAE-2. It also requires that all the unconstrained margins in the world were characterized by OAE-2-average OC MARs, while modern OC MARs characterized the abyssal environments. Perhaps increased OC production, preservation and burial in the Pacific Ocean could be explained by high(er) nutrient availability and enhanced preservation under low to absent oxygen conditions. In a general sense, the mapped MARs roughly mimic the modern patterns of OC burial, suggesting that OAE-2 was an amplification of processes observed in the modern oceans, particularly as related to broader ocean circulation patterns, upwelling and nutrient availability.

Understanding the global dynamics of the OC burial event during OAE-2 is key to interpreting the mechanisms that underlie the event, including the global redox state of the ocean and associated nutrient cycles and feedbacks. For example, increased carbon burial generally facilitates increased burial of reduced sulfur species (pyrite), which has been documented using sulfur isotopes ratios (Owens et al., 2013 and references therein). Iodine/calcium values and thallium isotopes suggest a global increase of anoxic water column conditions leading into and during the OAE (Ostrander et al., 2017; Zhou et al., 2017 and references therein), with the most reducing conditions at the onset of enhanced OC burial as suggested by S and Mo isotopes (Dickson et al., 2016a; Owens et al., 2013). Further, bio-essential trace-elements (Mo, V, Cr and Zn) are drawn down in euxinic settings during the event (Dickson et al., 2017; Owens et al., 2016, 2017 and references therein). The spread of low-oxygen, anoxic and euxinic conditions in the ocean and associated burial of organic carbon and pyrite can deplete the marine inventory of these metals, with profound implications for ecology and extinction patterns in the ancient oceans—and with possible relevance to de-oxygenation of other past, present and future warming oceans.

Acknowledgements

K. Choumiline, B. Gill, D. Hardisty, C. Reinhard, N. Riedinger, JP Trabucho Alexandre and T. Them provided helpful insights at various times in the project. This manuscript has benefited from reviews by Hugh Jenkyns, Karl Föllmi, an anonymous reviewer and editorial direction from Derek Vance. We thank the Agouron Institute (TWL and JDO), NSF-EAR 1338299 (TWL), NSF-OCE 1434785 (JDO), PRF-ACS 57545-ND2 (TWL), and NASA Exobiology NNX16AJ60 (JDO) for financial support.

Appendix A. Supplementary material

Supplementary material related to this article can be found online at https://doi.org/10.1016/j.epsl.2018.07.021.

References

Algeo, T.J., Lyons, T.W., 2006. Mo-total organic carbon covariation in modern anoxic marine environments: implications for analysis of paleoredox and paleohydrographic conditions. Paleoceanography 21, PA1016.

Arthur, M.A., Schlanger, S.O., Jenkyns, H.C., 1987. The Cenomanian–Turonian Oceanic Anoxic Event, II. Palaeoceanographic controls on organic-matter production and preservation. Geol. Soc. (Lond.) Spec. Publ. 26, 401–420.

Arthur, M.A., Dean, W.E., Pratt, L.M., 1988. Geochemical and climatic effects of increased marine organic carbon burial at the Cenomanian/Turonian boundary. Nature 335, 714–717.

Barclay, R.S., McElwain, J.C., Sageman, B.B., 2010. Carbon sequestration activated by a volcanic CO_2 pulse during Ocean Anoxic Event 2. Nat. Geosci. 3, 205–208.

Beerling, D., Berner, R.A., Mackenzie, F.T., Harfoot, M.B., Pyle, J.A., 2009. Methane and the CH_4 related greenhouse effect over the past 400 million years. Am. J. Sci. 309, 97–113.

Berner, R.A., 1990. Atmospheric carbon dioxide levels over Phanerozoic time. Science 249, 1382–1386.

Berner, R.A., Canfield, D.E., 1989. A new model for atmospheric oxygen over Phanerozoic time. Am. J. Sci. 289, 333–361.

Blumenberg, M., Wiese, F., 2012. Imbalanced nutrients as triggers for black shale formation in a shallow shelf setting during the OAE 2 (Wunstorf, Germany). Biogeosciences 9, 4139–4153.
Bralower, T.J., Thierstein, H.R., 1987. Organic carbon and metal accumulation rates in Holocene and mid-Cretaceous sediments: palaeoceanographic significance. Geol. Soc. (Lond.) Spec. Publ. 26, 345–369.
Brumsack, H.-J., 2006. The trace metal content of recent organic carbon-rich sediments: implications for Cretaceous black shale formation. Palaeogeogr. Palaeoclimatol. Palaeoecol. 232, 344–361.
Burdige, D.J., 2007. Preservation of organic matter in marine sediments: controls, mechanisms, and an imbalance in sediment organic carbon budgets? Chem. Rev. 107, 467–485.
Canfield, D.E., 1994. Factors influencing organic carbon preservation in marine sediments. Chem. Geol. 114, 315–329.
Charette, M.A., Smith, W.H.F., 2010. The volume of Earth's ocean. Oceanography 23, 112–114.
Dickson, A.J., Jenkyns, H.C., Porcelli, D., van den Boorn, S., Idiz, E., 2016a. Basin-scale controls on the molybdenum-isotope composition of seawater during Oceanic Anoxic Event 2 (Late Cretaceous). Geochim. Cosmochim. Acta 178, 291–306.
Dickson, A.J., Jenkyns, H.C., Porcelli, D., van den Boorn, S., Idiz, E., Owens, J.D., 2016b. Corrigendum to "Basin-scale controls on the molybdenum-isotope composition of seawater during Oceanic Anoxic Event 2 (Late Cretaceous)" [Geochim. Cosmochim. Acta 178 (2016) 291–306]. Geochim. Cosmochim. Acta 189, 404–405.
Dickson, A.J., Saker-Clark, M., Jenkyns, H.C., Bottini, C., Erba, E., Russo, F., Gorbanenko, O., Naafs, B.D.A., Pancost, R.D., Robinson, S.A., van den Boorn, S., Idiz, E., 2017. A Southern Hemisphere record of global trace-metal drawdown and orbital modulation of organic-matter burial across the Cenomanian–Turonian boundary (Ocean Drilling Program Site 1138, Kerguelen Plateau). Sedimentology 64, 186–203.
Du Vivier, A.D.C., Selby, D., Condon, D.J., Takashima, R., Nishi, H., 2015. Pacific $^{187}Os/^{188}Os$ isotope chemistry and U–Pb geochronology: synchroneity of global Os isotope change across OAE 2. Earth Planet. Sci. Lett. 428, 204–216.
Eldrett, J.S., Ma, C., Bergman, S.C., Lutz, B., Gregory, F.J., Dodsworth, P., Phipps, M., Hardas, P., Minisini, D., Ozkan, A., Ramezani, J., Bowring, S.A., Kamo, S.L., Ferguson, K., Macaulay, C., Kelly, A.E., 2015. An astronomically calibrated stratigraphy of the Cenomanian, Turonian and earliest Coniacian from the Cretaceous Western Interior Seaway, USA: implications for global chronostratigraphy. Cretac. Res. 56, 316–344.
Erbacher, J., Friedrich, O., Wilson, P.A., Birch, H., Mutterlose, J., 2005. Stable organic carbon isotope stratigraphy across Oceanic Anoxic Event 2 of Demerara Rise, western tropical Atlantic. Geochem. Geophys. Geosyst. 6, Q06010.
Föllmi, K.B., 2012. Early Cretaceous life, climate and anoxia. Cretac. Res. 35, 230–257.
Gill, B.C., Lyons, T.W., Young, S.A., Kump, L.R., Knoll, A.H., Saltzman, M.R., 2011. Geochemical evidence for widespread euxinia in the Later Cambrian ocean. Nature 469, 80–83.
Hartnett, H.E., Keil, R.G., Hedges, J.I., Decvol, A.H., 1998. Influence of oxygen exposure time on organic carbon preservation in continental margin sediments. Nature 391, 572–575.
Hasegawa, T., Crampton, J.S., Schiøler, P., Field, B., Fukushi, K., Kakizaki, Y., 2013. Carbon isotope stratigraphy and depositional oxia through Cenomanian/Turonian boundary sequences (Upper Cretaceous) in New Zealand. Cretac. Res. 40, 61–80.
Hayes, J.M., Strauss, H., Kaufman, A.J., 1999. The abundance of ^{13}C in marine organic matter and isotopic fractionation in the global biogeochemical cycle of carbon during the past 800 Ma. Chem. Geol. 161, 103–125.
Helly, J.J., Levin, L.A., 2004. Global distribution of naturally occurring marine hypoxia on continental margins. Deep-Sea Res., Part 1, Oceanogr. Res. Pap. 51, 1159–1168.
Hetzel, A., März, C., Vogt, C., Brumsack, H.-J., 2011. Geochemical environment of Cenomanian – Turonian black shale deposition at Wunstorf (northern Germany). Cretac. Res. 32, 480–494.
Jahnke, R.A., 1996. The global ocean flux of particulate organic carbon: areal distribution and magnitude. Glob. Biogeochem. Cycles 10, 71–88.
Jarvis, I.A.N., Murphy, A.M., Gale, A.S., 2001. Geochemistry of pelagic and hemipelagic carbonates: criteria for identifying systems tracts and sea-level change. J. Geol. Soc. 158, 685–696.
Jarvis, I., Gale, A.S., Jenkyns, H.C., Pearce, M.A., 2006. Secular variation in Late Cretaceous carbon isotopes: a new $\delta^{13}C$ carbonate reference curve for the Cenomanian–Campanian (99.6–70.6 Ma). Geol. Mag. 143, 561–608.
Jarvis, I., Lignum, J.S., Gröcke, D.R., Jenkyns, H.C., Pearce, M.A., 2011. Black shale deposition, atmospheric CO_2 drawdown, and cooling during the Cenomanian–Turonian Oceanic Anoxic Event. Paleoceanography 26, PA3201.
Jenkyns, H.C., 2010. Geochemistry of oceanic anoxic events. Geochem. Geophys. Geosyst. 11, Q03004.
Jobbágy, E.G., Jackson, R.B., 2000. The vertical distribution of soil organic carbon and its relation to climate and vegetation. Ecol. Appl. 10, 423–436.
Jones, C.E., Jenkyns, H.C., 2001. Seawater strontium isotopes, oceanic anoxic events, and seafloor hydrothermal activity in the Jurassic and Cretaceous. Am. J. Sci. 301, 112–149.
Jones, J., 2009. Technical note: total amounts of oil produced over the history of the industry. Int. J. Oil Gas Coal Tech. 2, 199–200.
Keller, G., Han, Q., Adatte, T., Burns, S.J., 2001. Palaeoenvironment of the Cenomanian–Turonian transition at Eastbourne, England. Cretac. Res. 22, 391–422.
Klemme, H., Ulmishek, G.F., 1991. Effective petroleum source rocks of the world: stratigraphic distribution and controlling depositional factors (1). Am. Assoc. Pet. Geol. Bull. 75, 1809–1851.
Kolonic, S., Wagner, T., Forster, A., Sinninghe Damsté, J.S., Walsworth-Bell, B., Erba, E., Turgeon, S., Brumsack, H.-J.r., Chellai, E.H., Tsikos, H., Kuhnt, W., Kuypers, M.M.M., 2005. Black shale deposition on the northwest African Shelf during the Cenomanian/Turonian oceanic anoxic event: climate coupling and global organic carbon burial. Paleoceanography 20, PA1006.
Kump, L.R., Arthur, M.A., 1999. Interpreting carbon-isotope excursions; carbonates and organic matter. Chem. Geol. 161, 181–198.
Kuroda, J., Ohkouchi, N., 2006. Implication of spatiotemporal distribution of black shales deposited during the Cretaceous oceanic anoxic event-2. Paleontol. Res. 10, 345–358.
Kurtz, A.C., Kump, L.R., Arthur, M.A., Zachos, J.C., Paytan, A., 2003. Early Cenozoic decoupling of the global carbon and sulfur cycles. Paleoceanography 18, 1090.
Kuypers, M.M.M., Pancost, R.D., Nijenhuis, I.A., Sinninghe Damsté, J.S., 2002. Enhanced productivity led to increased organic carbon burial in the euxinic North Atlantic basin during the late Cenomanian oceanic anoxic event. Paleoceanography 17, 1051.
Leckie, R.M., Bralower, T.J., Cashman, R., 2002. Oceanic anoxic events and plankton evolution: biotic response to tectonic forcing during the mid-Cretaceous. Paleoceanography 17, PA000623.
Miller, C.A., Peucker-Ehrenbrink, B., Walker, B.D., Marcantonio, F., 2011. Re-assessing the surface cycling of molybdenum and rhenium. Geochim. Cosmochim. Acta 75, 7146–7179.
Mort, H.P., Adatte, T., Föllmi, K.B., Keller, G., Steinmann, P., Matera, V., Berner, Z., Stüben, D., 2007. Phosphorus and the roles of productivity and nutrient recycling during oceanic anoxic event 2. Geology 35, 483–486.
Ostrander, C.M., Owens, J.D., Nielsen, S.G., 2017. Constraining the rate of oceanic deoxygenation leading up to a Cretaceous Oceanic Anoxic Event (OAE-2: ~94 Ma). Sci. Adv. 3.
Owens, J.D., Lyons, T.W., Li, X., Macleod, K.G., Gordon, G., Kuypers, M.M.M., Anbar, A., Kuhnt, W., Severmann, S., 2012. Iron isotope and trace metal records of iron cycling in the proto-North Atlantic during the Cenomanian–Turonian oceanic anoxic event (OAE-2). Paleoceanography 27, PA3223.
Owens, J.D., Gill, B.C., Jenkyns, H.C., Bates, S.M., Severmann, S., Kuypers, M.M.M., Woodfine, R.G., Lyons, T.W., 2013. Sulfur isotopes track the global extent and dynamics of euxinia during Cretaceous Oceanic Anoxic Event 2. Proc. Natl. Acad. Sci. 110, 18407–18412.
Owens, J.D., Reinhard, C.T., Rohrssen, M., Love, G.D., Lyons, T.W., 2016. Empirical links between trace metal cycling and marine microbial ecology during a large perturbation to Earth's carbon cycle. Earth Planet. Sci. Lett. 449, 407–417.
Owens, J.D., Lyons, T.W., Hardisty, D.S., Lowery, C.M., Lu, Z., Lee, B., Jenkyns, H.C., 2017. Patterns of local and global redox variability during the Cenomanian–Turonian Boundary Event (Oceanic Anoxic Event 2) recorded in carbonates and shales from central Italy. Sedimentology 64, 168–185.
Pogge von Strandmann, P.A.E., Jenkyns, H.C., Woodfine, R.G., 2013. Lithium isotope evidence for enhanced weathering during Oceanic Anoxic Event 2. Nat. Geosci. 6, 668–672.
Ronov, A.B., 1976. Global carbon geochemistry, volcanism, carbonate accumulation, and life [Translation of Geokhimiya]. Geochem. Int. 13, 172–195.
Sadler, P.M., 1981. Sediment accumulation rates and the completeness of stratigraphic sections. J. Geol. 89, 569–584.
Schlanger, S.O., Jenkyns, H.C., 1976. Cretaceous oceanic anoxic events: causes and consequences. Geol. Mijnb. 55, 179–184.
Schlanger, S.O., Arthur, M.A., Jenkyns, H.C., Scholle, P.A., 1987. The Cenomanian–Turonian Oceanic Anoxic Event, I. Stratigraphy and distribution of organic carbon-rich beds and the marine $\delta^{13}C$ excursion. In: Brooks, J., Fleet, A.J. (Eds.), Marine Petroleum Source Rocks. Geol. Soc. (Lond.) Spec. Publ. 26, 371–399.
Scholle, P.A., Arthur, M.A., 1980. Carbon isotope fluctuations in Cretaceous pelagic limestones; potential stratigraphic and petroleum exploration tool. Am. Assoc. Pet. Geol. Bull. 64, 67–87.
Schrag, D.P., Higgins, J.A., Macdonald, F.A., Johnston, D.T., 2013. Authigenic carbonate and the history of the global carbon cycle. Science 339, 540.
Scotese, C.R., 2008. The PALEOMAP Project PaleoAtlas for ArcGIS, vol. 2. Cretaceous Paleogeographic and Plate Rectonic Reconstructions. PALEOMAP Project.
Scott, C., Lyons, T.W., 2012. Contrasting molybdenum cycling and isotopic properties in euxinic versus non-euxinic sediments and sedimentary rocks: refining the paleoproxies. Chem. Geol. 324–325, 19–27.
Smith, M.A., 1990. Lacustrine Oil Shale in the Geologic Record. Chapter 3.
Takashima, R., Nishi, H., Huber, B.T., Leckie, M., 2006. Greenhouse World and the Mesozoic Ocean. Oceanography 19, 82–92.
Them, T.R., Gill, B.C., Caruthers, A.H., Gerhardt, A.M., Gröcke, D.R., Lyons, T.W., Marroquín, S.M., Nielsen, S.G., Trabucho Alexandre, J.P., Owens, J.D., 2018. Thallium isotopes reveal protracted anoxia during the Toarcian (Early Jurassic) associated with volcanism, carbon burial, and mass extinction. Proc. Natl. Acad. Sci. https://doi.org/10.1073/pnas.1803478115.

Trabucho Alexandre, J., Tuenter, E., Henstra, G.A., van der Zwan, K.J., van de Wal, R.S.W., Dijkstra, H.A., de Boer, P.L., 2010. The mid-Cretaceous North Atlantic nutrient trap: black shales and OAEs. Paleoceanography 25, PA4201.

Turgeon, S.C., Creaser, R.A., 2008. Cretaceous oceanic anoxic event 2 triggered by a massive magmatic episode. Nature 454, 323–326.

van Bentum, E.C., Hetzel, A., Brumsack, H.-J., Forster, A., Reichart, G.-J., Sinninghe Damsté, J.S., 2009. Reconstruction of water column anoxia in the equatorial Atlantic during the Cenomania–Turonian oceanic anoxic event using biomarker and trace metal proxies. Palaeogeogr. Palaeoclimatol. Palaeoecol. 280, 489–498.

van Bentum, E.C., Reichart, G.-J., Forster, A., Sinninghe Damsté, J.S., 2012. Latitudinal differences in the amplitude of the OAE-2 carbon isotopic excursion: pCO_2 and paleo productivity. Biogeosciences 9, 717–731.

Van Cappellen, P., Ingall, E.D., 1994. Benthic phosphorus regeneration, net primary production, and ocean anoxia: a model of the coupled marine biogeochemical cycles of carbon and phosphorus. Paleoceanography 9, 677–692.

Weissert, H., Lini, A., Föllmi, K.B., Kuhn, O., 1998. Correlation of Early Cretaceous carbon isotope stratigraphy and platform drowning events: a possible link? Palaeogeogr. Palaeoclimatol. Palaeoecol. 137, 189–203.

Westermann, S., Föllmi, K.B., Adatte, T., Matera, V., Schnyder, J., Fleitmann, D., Fiet, N., Ploch, I., Duchamp-Alphonse, S., 2010. The Valanginian $\delta^{13}C$ excursion may not be an expression of a global oceanic anoxic event. Earth Planet. Sci. Lett. 290, 118–131.

Xu, W., Ruhl, M., Jenkyns, H.C., Hesselbo, S.P., Riding, J.B., Selby, D., Naafs, B.D.A., Weijers, J.W.H., Pancost, R.D., Tegelaar, E.W., Idiz, E.F., 2017. Carbon sequestration in an expanded lake system during the Toarcian oceanic anoxic event. Nat. Geosci. 10, 129–134.

Zhou, X., Jenkyns, H.C., Lu, W., Hardisty, D.S., Owens, J.D., Lyons, T.W., Lu, Z., 2017. Organically bound iodine as a bottom-water redox proxy: preliminary validation and application. Chem. Geol. 457, 95–106.